Vaibhav B. Patel,[1,2] Jun Mori,[2,3] Brent A. McLean,[2,4] Ratnadeep Basu,[1,2] Subhash K. Das,[1,2] Tharmarajan Ramprasath,[1,2] Nirmal Parajuli,[1,2] Josef M. Penninger,[5] Maria B. Grant,[6] Gary D. Lopaschuk,[2,3] and Gavin Y. Oudit[1,2,4,7]

ACE2 Deficiency Worsens Epicardial Adipose Tissue Inflammation and Cardiac Dysfunction in Response to Diet-Induced Obesity

Diabetes 2016;65:85–95 | DOI: 10.2337/db15-0399

Obesity is increasing in prevalence and is strongly associated with metabolic and cardiovascular disorders. The renin-angiotensin system (RAS) has emerged as a key pathogenic mechanism for these disorders; angiotensin (Ang)-converting enzyme 2 (ACE2) negatively regulates RAS by metabolizing Ang II into Ang 1-7. We studied the role of ACE2 in obesity-mediated cardiac dysfunction. ACE2 null (ACE2KO) and wild-type (WT) mice were fed a high-fat diet (HFD) or a control diet and studied at 6 months of age. Loss of ACE2 resulted in decreased weight gain but increased glucose intolerance, epicardial adipose tissue (EAT) inflammation, and polarization of macrophages into a proinflammatory phenotype in response to HFD. Similarly, human EAT in patients with obesity and heart failure displayed a proinflammatory macrophage phenotype. Exacerbated EAT inflammation in ACE2KO-HFD mice was associated with decreased myocardial adiponectin, decreased phosphorylation of AMPK, increased cardiac steatosis and lipotoxicity, and myocardial insulin resistance, which worsened heart function. Ang 1-7 (24 μg/kg/h) administered to ACE2KO-HFD mice resulted in ameliorated EAT inflammation and reduced cardiac steatosis and lipotoxicity, resulting in normalization of heart failure. In conclusion, ACE2 plays a novel role in heart disease associated with obesity wherein ACE2 negatively regulates obesity-induced EAT inflammation and cardiac insulin resistance.

Obesity is a growing worldwide health problem and results in an increased health care burden and a decreased life expectancy. Obesity itself is an independent risk factor for the development of heart failure with preserved ejection fraction (HFPEF) independent of other comorbid conditions (1–4). Although a number of mechanisms are speculated to contribute to obesity-induced cardiac dysfunction, including lipotoxicity, inflammation, mitochondrial dysfunction, endoplasmic reticulum stress, and apoptosis, the ultimate cause and mechanisms remain elusive (5–7). Clinical and experimental evidence has revealed a key role of excessive fat in the onset of obesity and accompanying inflammation and cardiac dysfunction.

Components of the renin-angiotensin system (RAS) are present in white and brown adipose tissues where the local RAS can be pathogenic (8). The angiotensin type 1 and type 2 receptors (AT1Rs and AT2Rs, respectively) may mediate the effect of angiotensin (Ang) II and cause upregulation of adipose tissue lipogenesis (mediated through AT2R) and downregulation of lipolysis (mediated through AT1R) (9,10). Ang-converting enzyme 2 (ACE2) is a central member of the RAS family that degrades Ang II into Ang 1-7 (11,12). Ang 1-7 is a biologically active product of the Ang II degradation that through the activation of Mas receptors leads to vasodilatory, antihypertrophic, and antifibrotic effects (13–16). ACE2 is widely distributed in various organs and cell types, including adipocytes (17).

[1]Division of Cardiology, Department of Medicine, University of Alberta, Edmonton, Alberta, Canada
[2]Mazankowski Alberta Heart Institute, University of Alberta, Edmonton, Alberta, Canada
[3]Departments of Pediatrics and Pharmacology, University of Alberta, Edmonton, Alberta, Canada
[4]Department of Physiology, University of Alberta, Edmonton, Alberta, Canada
[5]Institute of Molecular Biotechnology of the Austrian Academy of Sciences, Vienna, Austria
[6]Department of Ophthalmology, Indiana University School of Medicine, Indianapolis, IN
[7]Alberta Diabetes Institute, University of Alberta, Edmonton, Alberta, Canada

Corresponding author: Gavin Y. Oudit, gavin.oudit@ualberta.ca.

Received 25 March 2015 and accepted 20 July 2015.

This article contains Supplementary Data online at http://diabetes.diabetesjournals.org/lookup/suppl/doi:10.2337/db15-0399/-/DC1.

See accompanying article, p. 19.

It is a negative regulator of the activated RAS in various disease states, including heart failure, diabetic nephropathy and cardiomyopathy, and vascular dysfunction (18–21). In this study, we determined a novel role of ACE2 in adipose tissue inflammation and its effects on cardiac function in diet-induced obesity (DIO).

RESEARCH DESIGN AND METHODS

Experimental Animals and Protocols

$Ace2^{-/y}$ mutant mice (ACE2KO) backcrossed into the C57BL/6 background for at least eight generations were used in the current study (18,21,22). All experiments were performed in accordance with University of Alberta institutional guidelines, which conform to guidelines published by the Canadian Council on Animal Care and the Guide for the Care and Use of Laboratory Animals published by the U.S. National Institutes of Health (revised 2011). Male wild-type (WT) and ACE2KO mice were fed either a high-fat diet (HFD) (45% kilocalories from fat) or a control diet (CON) (10% kilocalories from fat) from weaning to 6 months of age. ALZET microosmotic pumps (Model 1002; DURECT Corporation) were implanted subcutaneously in ACE2KO-HFD mice to deliver Ang 1-7 (24 μg/kg/h) or saline (control) for 4 weeks (21). All mice were studied at 6 months of age. Epicardial adipose tissues (EATs) were collected under a stereo microscope after removal of the pericardium and pericardial fat.

Human EAT

Human EAT obtained from explanted nonobese, nonfailing control (NFC) hearts and diseased hearts from obese (BMI >30 kg/m^2) patients with HFPEF secondary to hypertension or transplant vasculopathy was studied as part of the Human Explanted Heart Program (HELP) at the Mazankowski Alberta Heart Institute and the Human Organ Procurement and Exchange (HOPE) program at the University of Alberta Hospital. All experiments were performed in accordance with institutional guidelines and were approved by the institutional ethics committee. Informed consent was obtained from all participants.

Intraperitoneal Glucose Tolerance Test

An intraperitoneal glucose tolerance test was performed on overnight-fasted mice (16 h). Briefly, mice were administered glucose 1 g/kg i.p., and blood glucose levels were monitored at 0, 15, 30, 60, 90, and 120 min postglucose administration and plotted against time curves to determine the glucose tolerance (13).

Echocardiography, Pressure-Volume Loop Analysis, and Quantitative Magnetic Resonance

Transthoracic echocardiography was performed noninvasively to assess systolic and diastolic function as described previously using a Vevo 770 high-resolution imaging system equipped with a 30-MHz transducer (RMV707B; VisualSonics, Toronto, Ontario, Canada) (13,18). Mice were placed on a heating pad, and a nose cone with 1.5% isoflurane in 100% oxygen was applied. Temperature was maintained at 36.5–37.5°C. Ultrasound gel was placed on the chest of the anesthetized mouse. The temperature and heart rate were constantly monitored during the scanning. M-mode images were obtained for measurements of left ventricular (LV) ejection fraction. Transmitral flow and tissue Doppler imaging were used to assess the E/A ratio and E/E′ ratios. LV pressure-volume relationships were assessed using a 1.2-F admittance catheter (Scisense Inc.) as previously described (13). The position of the catheter was monitored by pressure along with the magnitude and phase using the ADVantage Pressure-Volume System (Scisense Inc.) and iWorx (iWorx Systems, Inc.). Online as well as offline calculations were performed using LabScribe2 version 2.347000 software. Body composition (either fat mass or lean mass) was assessed using an EchoMRI-900 (EchoMRI LLC, Houston, TX) as previously reported (13).

Isolated Working Heart Perfusion

At the end of the protocol, isolated hearts were perfused in a working mode at a left atrial preload of 11.5 mmHg and an aortic afterload of 50 mmHg as previously reported (13). The perfusate contained 2.5 mmol/L Ca^{2+}, 5 mmol/L [U-^{14}C]glucose, and 1.2 mmol/L [9,10-^{3}H]palmitate prebound to 3% fatty acid–free BSA. We used a higher concentration of palmitate to simulate the physiological fatty acid levels in HFD-fed mice. Hearts underwent aerobic perfusion in the absence of insulin for the first 30 min, and then 100 μU/mL insulin was added to the perfusate to examine the response to insulin. Glucose oxidation or palmitate oxidation rates were measured by quantitative collection of $^{14}CO_2$ and $^{3}H_2O$ from [U-^{14}C]glucose and [9,10-^{3}H]palmitate, respectively. Glucose-derived and palmitate-derived ATP production rates were calculated from the rates of glucose oxidation and palmitate oxidation.

Histological and Immunofluorescence Analyses, Oil Red O Staining, Western Blot Analysis, and TaqMan Real-Time PCR

Mouse and human EAT and mouse hearts were studied using histology, immunofluorescence (IF) staining, wheat germ agglutinin (WGA) staining (to delineate the cell membrane), confocal imaging, Western blot analyses, and TaqMan real-time PCR molecular analyses, as previously described (13,18,20). Picrosirius red staining was performed on the 10-μm-thick formalin-fixed paraffin-embedded sections to assess cardiac fibrosis as previously described (18,23). Oil Red O staining was carried out on 5-μm-thick optimal cutting temperature–embedded cryosections as previously described (13).

Tumor Necrosis Factor-α ELISA

ELISA was carried out in the EAT to assess tumor necrosis factor-α (TNF-α) protein levels using a commercially available kit (R&D Systems) as previously described (24). Briefly, 50 μg of the total proteins isolated from the pooled EAT was used to assess TNF-α levels using the murine recombinant TNF-α as standard. The plates were analyzed with a multiplate reader (SpectraMax).

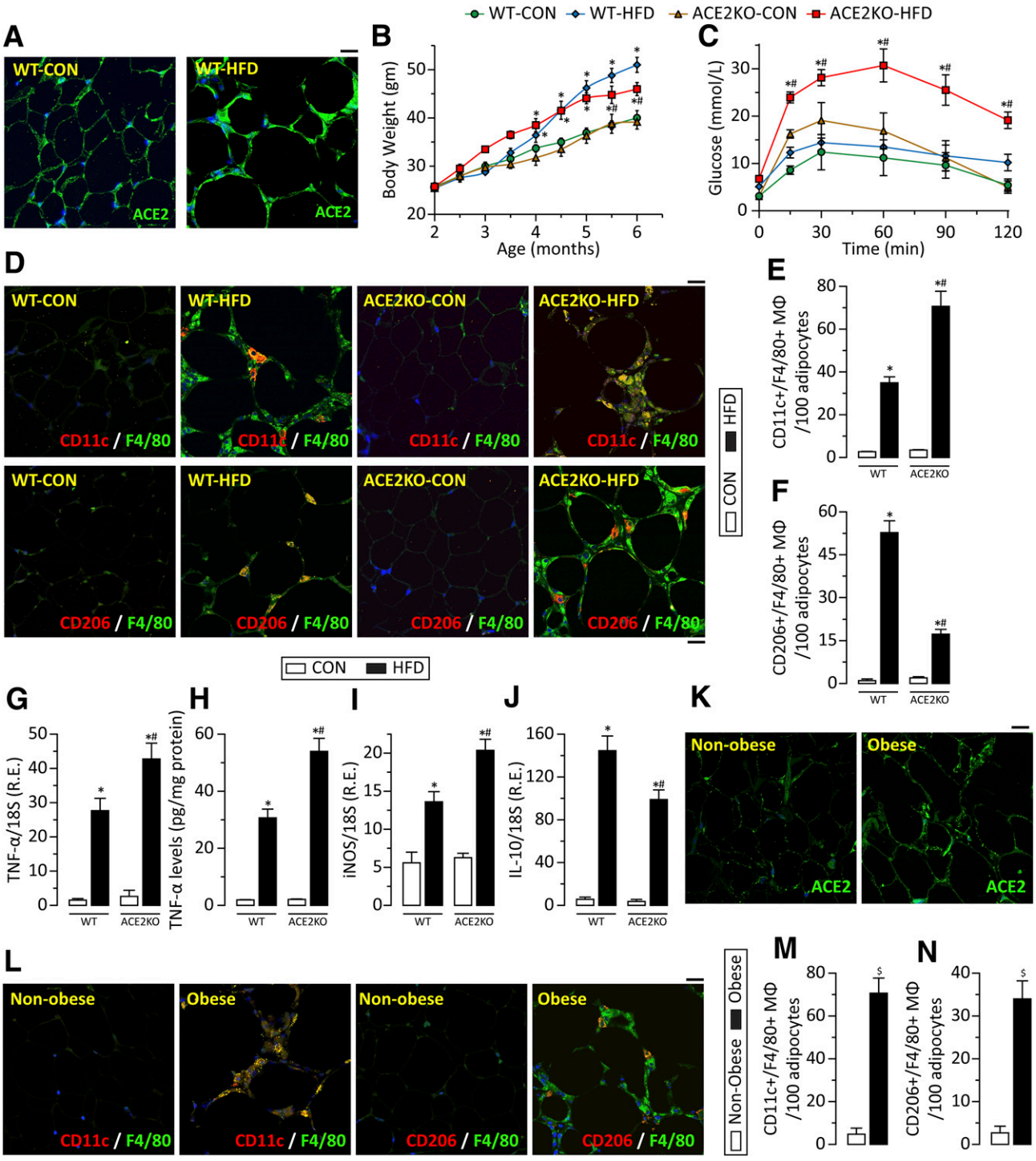

Figure 1—ACE2 is upregulated in EAT in response to DIO, whereas loss of ACE2 results in increased DIO-induced EAT inflammation. Representative IF images show increased adipocyte ACE2 expression in response to DIO (*A*). Body weight changes in WT and ACE2KO mice in response to CON and HFD show decreased body weight gain in ACE2KO-HFD mice compared with WT-HFD mice (*B*). Intraperitoneal glucose tolerance test in fasted mice shows increased glucose intolerance in ACE2KO-HFD mice (*C*). Representative IF images for F4/80 and CD11c and CD206 (*D*) show markedly increased inflammation in ACE2KO-HFD EAT. WT-HFD shows increased resident CD206$^+$ anti-inflammatory Mϕ, whereas ACE2KO-HFD shows polarization in the Mϕ phenotype, resulting in increased CD11c$^+$ proinflammatory Mϕ (*D–F*). Gene expression analysis and ELISA show a greater increase in TNF-α [mRNA (*G*) and protein levels (*H*)] and iNOS (*I*) mRNA expression and a lesser increase in IL-10 (*J*) mRNA expression in ACE2KO-HFD EAT compared with WT-HFD. Representative IF images show increased adipocyte ACE2 expression in obese patients with HFPEF compared with nonobese NFC subjects (*K*). Representative IF images for F4/80 and CD11c and CD206 in the human adipose tissue show markedly increased CD11c$^+$ Mϕ with a smaller increase in CD206$^+$ Mϕ in EAT of human explanted hearts from obese patients with HFPEF (*L–N*). n = 4 (*A*, *D–F*, *K*, *L*); n = 20 (*B*); n = 8 (*C*, *H*); n = 12 (*G*, *I*, *J*). *P < 0.05 compared with the respective CON groups; #P < 0.05 compared with WT-HFD group; $$P$ < 0.05 compared with the nonobese NFC group. Scale bar = 25 μm. R.E., relative expression.

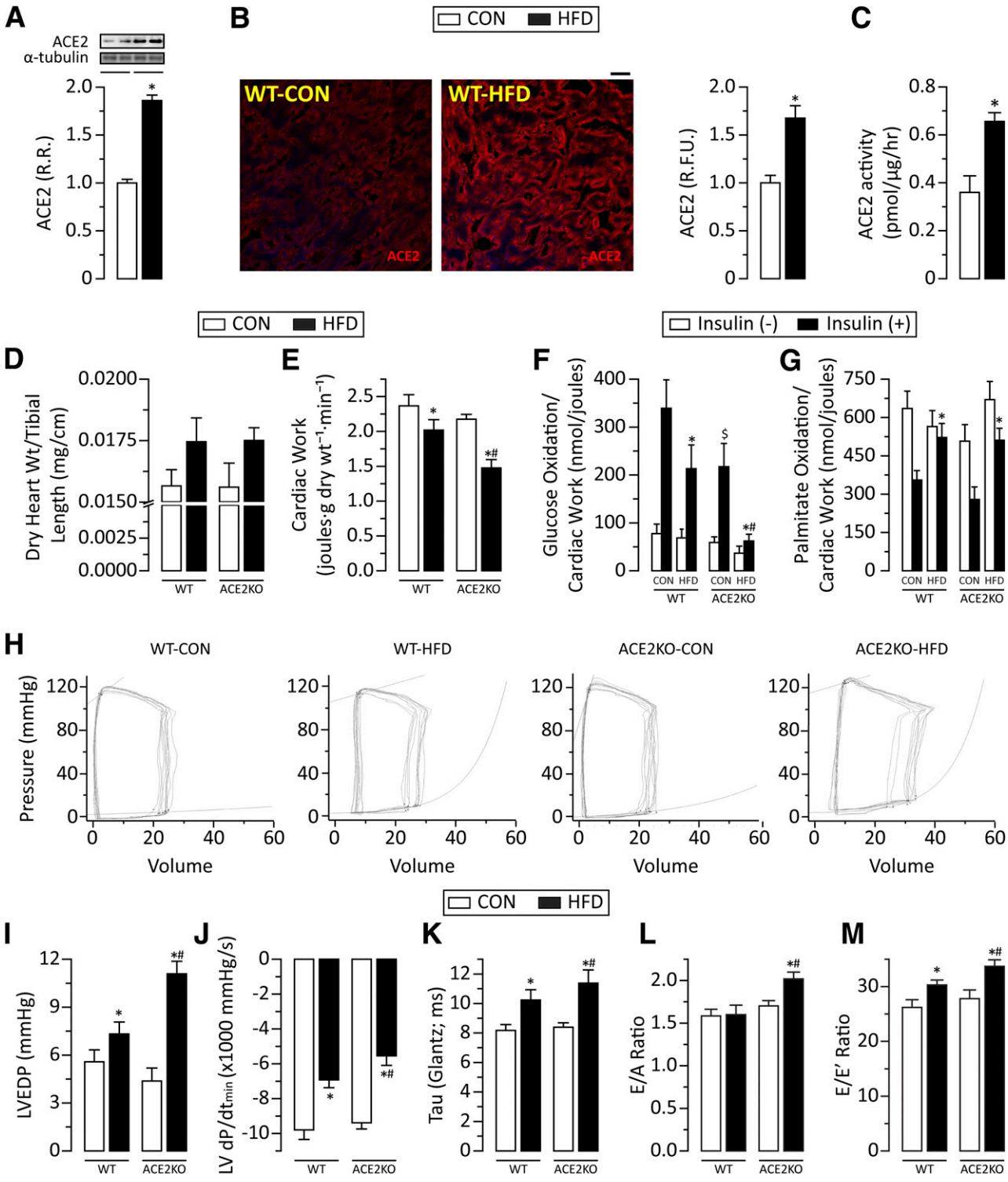

Figure 2—ACE2 is upregulated in the myocardium in response to DIO, but loss of ACE2 results in worsened cardiac insulin resistance and heart failure. Western blot analysis (*A*), representative IF staining images and quantification (*B*), and ACE2 activity assay (*C*) show myocardial ACE2 upregulation in response to DIO. Ratio of dry heart weight to tibial length shows equivalent cardiac hypertrophy in the WT-HFD and ACE2KO-HFD groups (*D*). Ex vivo working heart perfusions show decreased cardiac work in ACE2KO-HFD hearts compared with WT-HFD hearts (*E*). Rates of glucose oxidation determined by ex vivo working heart perfusions show an insulin-induced increase in glucose oxidation in WT-CON hearts (*F*). WT-HFD and ACE2KO-CON hearts show a decreased effect of insulin on glucose oxidation, which was entirely blunted in ACE2KO-HFD hearts. Ex vivo working heart perfusions showing decreased palmitate oxidation rate in response to insulin perfusion in WT-CON and ACE2KO-CON hearts with further equivalent reductions in WT-HFD and ACE2KO-HFD hearts (*G*). Pressure-volume loop (*H*) analysis shows a greater increase in LVEDP (*I*) in ACE2KO-HFD mice, which is associated with a greater slowing of cardiac relaxation shown by decreased LV dP/dt_{min} (*J*) and Tau (Glantz) (*K*). Echocardiographic analysis of transmitral flow pattern and tissue Doppler imaging show a greater increase in E/A ratio (*L*) and E/E′ ratio (*M*) in ACE2KO-HFD mice compared with WT-HFD mice. $n = 6$ (*A*); $n = 4$ (*B*);

Statistical Analysis

All data are presented as mean ± SEM. All statistical analyses were performed using SPSS version 22 software (IBM Corporation, Chicago, IL). Between-group comparisons were made using a nonpaired Student *t* test. The effects of genotype and HFD were evaluated using one-way ANOVA followed by the Student-Neuman-Keuls test for multiple-comparison testing. In experiments with multiple treatments, one-way ANOVA was followed by multiple comparisons using the Student-Neuman-Keuls test. Statistical significance is recognized at $P < 0.05$.

RESULTS

Loss of ACE2 Increased EAT Inflammation in DIO

A marked upregulation of ACE2 was observed in the EAT from WT mice subjected to DIO (Fig. 1*A*). Growth curves and assessment of body composition (analyzed by quantitative magnetic resonance) showed that ACE2KO-HFD mice had a smaller gain in total body weight and total fat mass (Fig. 1*B* and Supplementary Fig. 1*A* and *B*) without a differential effect on body composition as illustrated by an equivalent increase in fat (Supplementary Fig. 1*C*) and lean (Supplementary Fig. 1*D*) mass compositions compared with WT-HFD mice. Despite the reduced obesity, ACE2KO-HFD mice showed a greater increase in fasting plasma glucose (Supplementary Fig. 1*E*) and increased glucose intolerance (Fig. 1*C* and Supplementary Fig. 1*F*) compared with WT-HFD mice. The results are consistent with the previous observation of impaired glucose intolerance in ACE2KO mice in response to a high-calorie diet (25).

Adipose tissue inflammation is linked to obesity-induced insulin resistance (26). Although HFD feeding resulted in an equivalent increase in EAT mass in WT and ACE2KO mice (Supplementary Fig. 1*G*), histological analysis by hematoxylin-eosin staining (Supplementary Fig. 2*A*) and WGA staining (Supplementary Fig. 2*B*) showed an uncoupling between obesity and adipose tissue inflammation in ACE2KO-HFD EAT. Despite the reduced obesity in ACE2KO-HFD mice, EAT showed increased inflammatory cell infiltration (Supplementary Fig. 2*A*), crown-like structures (Supplementary Fig. 2*C*), and adipocyte area (Supplementary Fig. 2*B* and *D*). The increased crown-like structures in the EAT of ACE2KO-HFD mice suggests advanced inflammation and increased adipocyte necrosis (27). IF staining for macrophage (Mϕ) cell markers, including the F4/80 (Mϕ cell-surface marker), CD11c [marker for the proinflammatory phenotype of Mϕ that resembles M(interferon-γ [IFN-γ]) Mϕ], and CD206 [marker for the anti-inflammatory phenotype of Mϕ that resembles M(interleukin-4 [IL-4]) Mϕ], was carried out (Fig. 1*D*) to characterize the phenotypes of Mϕ in EAT (28,29). The EAT of WT-HFD displayed a smaller increase in the $CD11c^+/F4/80^+$ and a greater increase in the $CD206^+/F4/80^+$ phenotypes of Mϕ based on IF staining (Fig. 1*D–F*). In contrast, EAT of ACE2KO-HFD showed polarization of the Mϕ phenotype, resulting in increased $CD11c^+/F4/80^+$ and decreased $CD206^+/F4/80^+$ phenotypes of Mϕ (Fig. 1*D–F*) compared with WT-HFD. Correspondingly, the mRNA expression profile of ACE2KO-HFD EAT showed a greater increase in the expression of proinflammatory cytokine TNF-α, resulting in increased TNF-α protein levels in ACE2KO-HFD EAT (Fig. 1*G* and *H*). Gene expression analysis also showed a greater increase in M(IFN-γ)-associated inducible nitric oxide synthase (iNOS), MCP-1, IL-1β, and IL-6 (Fig. 1*I* and Supplementary Fig. 1*E* and *F*) and a lesser increase in M(IL-4)-associated anti-inflammatory cytokine IL-10 (Fig. 1*J*) mRNA expression in ACE2KO-HFD EAT compared with WT-HFD EAT.

We also found increased ACE2 in EAT obtained from the obese patients with HFPEF compared with the nonobese NFC patients (Fig. 1*K*). BMI was 25.3 ± 1.6 (n = 6) and 36.7 ± 2.1 (n = 6) kg/m^2 ($P < 0.05$) in the nonobese NFC and obese patients with HFPEF, respectively. IF staining revealed increased resident Mϕ in EAT obtained from explanted diseased hearts from obese patients (Fig. 1*L*). Of note, the Mϕ in EAT from obese patients showed a greater increase in the $CD11c^+/F4/80^+$ phenotype than in the $CD206^+/F4/80^+$ phenotype (Fig. 1*L–N*). These results illustrate that ACE2 plays a dominant role in suppressing EAT inflammation and in maintaining glucose tolerance in the setting of obesity.

ACE2 Deficiency Worsened Cardiac Insulin Resistance, Resulting in HFPEF

We next examined the effects of increased EAT inflammation on HFPEF. Western blot analysis (Fig. 2*A*), IF staining (Fig. 2*B*), and activity assay (Fig. 2*C*) showed upregulation of myocardial ACE2 in WT mice in response to DIO. DIO resulted in equivalent pathological hypertrophy in WT and ACE2KO mice (Fig. 2*D*). Conversely, loss of ACE2 resulted in decreased cardiac work when assessed by ex vivo working heart perfusions (Fig. 2*E*). In WT-CON hearts, perfusion with insulin resulted in a marked increase in glucose oxidation (Fig. 2*F*). This increase was suppressed in WT-HFD and ACE2KO-CON hearts, with ACE2KO-HFD hearts showing a severely blunted response to insulin. Myocardial palmitate oxidation in WT and ACE2KO hearts was similarly decreased in response to insulin (Fig. 2*G*) with an equivalent loss of sensitivity to

n = 8 (*C*); n = 12 (*D–G*, *L*, *M*); n = 10 (*H–K*). *$P < 0.05$ compared with the respective CON groups; #$P < 0.05$ compared with WT-HFD group; \$$P < 0.05$ compared with WT-CON group. Scale bar = 25 μm. LV dP/dt_{min}, rate of LV pressure decrease; R.F.U., relative fluorescence unit; R.R., relative ratio; Tau (Glantz), exponential decay of the ventricular pressure during isovolumic relaxation; wt, weight.

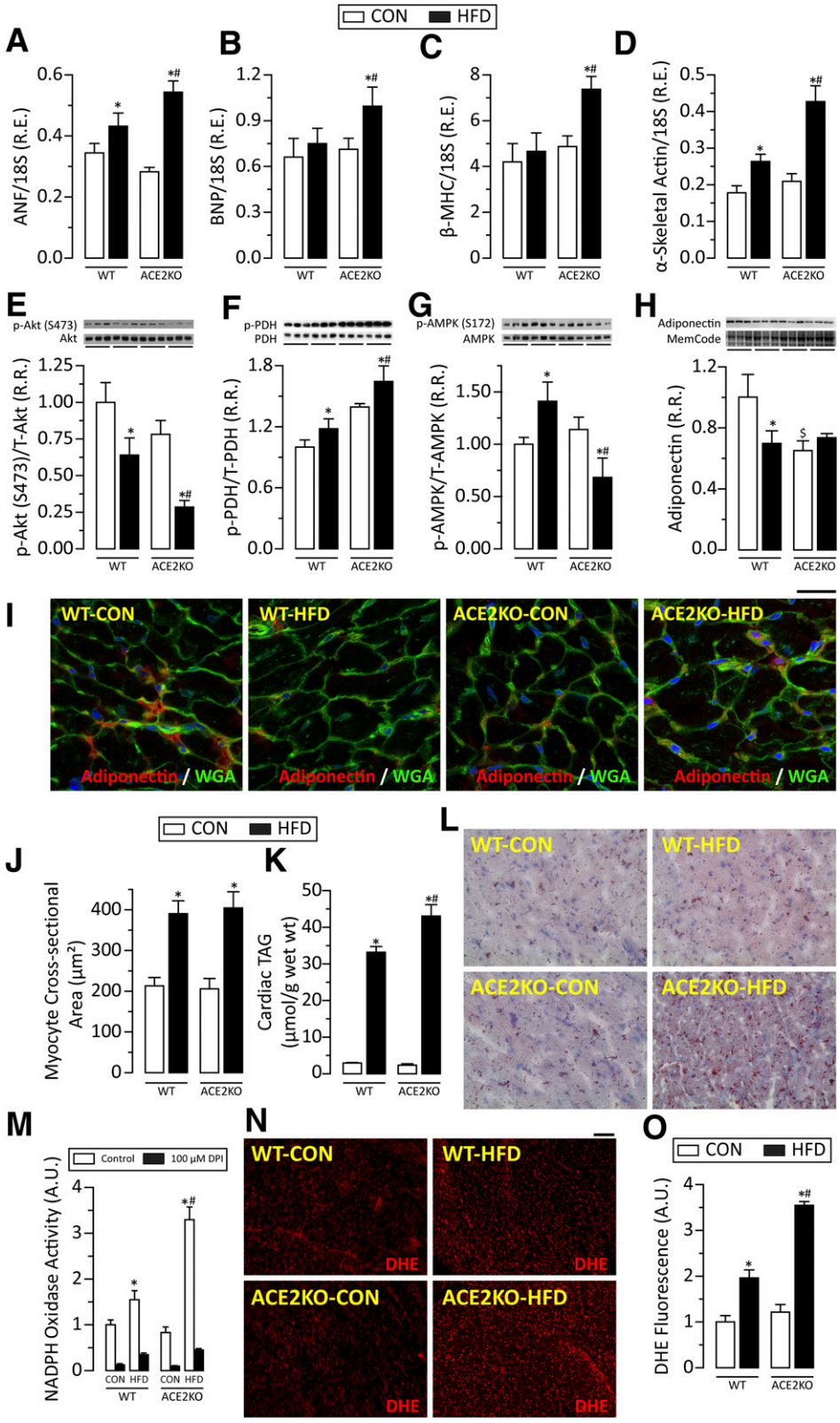

Figure 3—Loss of ACE2 results in cardiac steatosis, oxidative stress, and modulation of molecular signaling pathways in response to DIO. Increased mRNA expression of ANF (*A*), BNP (*B*), β-MHC (*C*), and α-skeletal actin (*D*) shows heart failure progression in ACE2KO-HFD hearts in response to DIO. Western blot analysis shows a greater decrease in phosphorylation of Akt in ACE2KO-HFD hearts compared with WT-HFD hearts (*E*). Phosphorylation of PDH was increased in WT-HFD hearts and further increased in ACE2KO-HFD hearts (*F*). Phosphorylation of AMPK was increased in WT-HFD hearts but decreased in ACE2KO-HFD hearts (*G*). Western blot analysis (*H*) and representative IF images (*I*) show decreased adiponectin levels in WT-HFD hearts. ACE2KO-CON hearts showed reduced basal levels of myocardial adiponectin, which remained low in response to DIO. Representative WGA-stained images (*I*) and myocyte cross-sectional area

insulin in both genotypes with DIO (Fig. 2*G*). Assessment of total ATP (Supplementary Fig. 3*A*) and percent ATP production (Supplementary Fig. 3*B*) showed that ATP production originating from glucose oxidation was stimulated by insulin in WT-CON and ACE2KO-CON hearts but was partially and almost completely suppressed in WT-HFD and ACE2KO-HFD hearts, respectively. LV pressure-volume analysis (Fig. 2*H*) showed worsened diastolic dysfunction, as illustrated by a greater increase in LV end-diastolic pressure (LVEDP) (Fig. 2*I*) with preserved systolic function (Supplementary Fig. 3*C*) in ACE2KO-HFD mice than in WT-HFD mice. Worsened diastolic dysfunction in the ACE2KO-HFD mice was mainly a result of the impaired active relaxation, as evidenced by a greater decrease in the LV dP/dt_{min} (Fig. 2*J*) and increased Tau (Fig. 2*K* and Supplementary Fig. 3*D*), the exponential time constant of the decay in LV pressure during isovolumic relaxation, coupled with an equivalent increase in passive stiffness as reflected in the end-diastolic pressure-volume relationship (EDPVR) (Supplementary Fig. 3*E*). Transmitral flow and tissue Doppler imaging revealed markedly increased E/A and E/E′ ratios consistent with diastolic dysfunction in the ACE2KO-HFD mice (Fig. 2*L* and *M*). The mRNA expression profile of molecular markers of cardiac diseases showed a greater increase in the expression of atrial natriuretic factor (ANF) (Fig. 3*A*), brain natriuretic peptide (BNP) (Fig. 3*B*), β-myosin heavy chain (β-MHC) (Fig. 3*C*), and α-skeletal muscle actin (Fig. 3*D*) in ACE2KO-HFD hearts compared with WT-HFD hearts. These results clearly demonstrate that loss of ACE2 enhances the susceptibility of the heart to obesity-induced heart disease.

Molecular Mechanism of the Cardiac Insulin Resistance and HFPEF in ACE2KO-HFD Hearts

Western blot analyses of various metabolic enzymes and metabolic signaling pathways (30,31) were carried out in the insulin-perfused hearts to elucidate the mechanism of myocardial insulin resistance in ACE2KO-HFD hearts. Of note, insulin-mediated phosphorylation of Akt was decreased in the WT-HFD hearts, a response further exacerbated in ACE2KO-HFD hearts, suggesting a marked cardiac insulin resistance in DIO in ACE2-deficient mice (Fig. 3*E*). Decreased phosphorylation of Akt in ACE2KO-HFD hearts was associated with increased pyruvate dehydrogenase kinase (PDK) 4 protein levels (Supplementary Fig. 4*A*), with no difference in PDK2 levels (Supplementary Fig. 4*B*), and increased phosphorylation of pyruvate dehydrogenase (PDH) (Fig. 3*F*), a rate-limiting enzyme in carbohydrate oxidation. Phosphorylation of AMPK was increased in WT-HFD hearts, whereas ACE2KO-HFD hearts showed decreased phosphorylation of AMPK (Fig. 3*G*). We assessed myocardial levels of adiponectin, an adipokine that regulates inflammation and cardiac metabolism (32,33). Western blot and IF analyses showed decreased myocardial adiponectin levels in WT hearts in response to DIO (Fig. 3*H* and *I*). ACE2KO-CON hearts showed reduced basal levels of myocardial adiponectin, which remained low in response to DIO (Fig. 3*H* and *I*), whereas the increase in cardiomyocyte cross-sectional area was equivalent in WT and ACE2KO mice in response to HFD feeding (Fig. 3*J*).

There was no difference in the protein levels of sirtuin (SIRT)-1 and SIRT-4 (Supplementary Fig. 4*C* and *D*), whereas SIRT-3 protein levels were decreased (Supplementary Fig. 4*E*) and peroxisome proliferator–activated receptor γ coactivator protein levels were increased (Supplementary Fig. 4*F*) in WT-HFD, ACE2KO-CON, and ACE2KO-HFD hearts compared with WT-CON hearts. In addition, other than reduction in the ACE levels in WT hearts in response to DIO, there was no noticeable difference in the protein levels of AT1R, ACE, and Mas receptor in WT and ACE2KO hearts (Supplementary Fig. 4*G–I*). Obesity is closely linked to cardiac steatosis and lipotoxicity, which are key pathogenic events in driving heart disease in obese states (26,34). Myocardial triacylglycerol (TAG) levels showed a marked increase in ACE2KO-HFD hearts compared with WT-HFD hearts (Fig. 3*K*) as confirmed by Oil Red O staining, which showed markedly increased myocardial lipid accumulation in ACE2KO-HFD hearts (Fig. 3*L*). Increased cardiac steatosis was associated with increased oxidative stress as shown by increased NADPH oxidase activity (Fig. 3*M*) and dihydroethidium (DHE) fluorescence (Fig. 3*N* and *O*), predisposing the ACE2KO-HFD hearts to lipotoxicity. There was no difference in the mRNA expression of proinflammatory cytokines, including TNF-α, MCP-1, and IL-6, and an equivalent increase in IL-1β between the ACE2KO-HFD and WT-HFD hearts (Supplementary Fig. 5*A–D*). Picrosirius red staining showed an equivalent increase in myocardial fibrosis in ACE2KO-HFD hearts compared with WT-HFD hearts, which was consistent with the equivalent increase in passive stiffness (EDPVR) (Supplementary Fig. 5*E* and *F*).

Ang 1-7 Treatment Decreased EAT Inflammation, Corrected Signaling Pathways and Lipotoxicity, and Rescued Heart Disease in ACE2KO-HFD Mice

Ang 1-7 treatment for 4 weeks reduced DIO-induced glucose intolerance in ACE2KO mice (Supplementary Fig. 6*A* and *B*) without affecting body weight (Supplementary Fig. 6*C*).

(*J*) show equivalent cardiac hypertrophy in WT-HFD and ACE2KO-HFD mice. Biochemical analysis showed increased cardiac TAG levels (*K*), and Oil Red O staining showed increased intramyocardial lipid accumulation (*L*) in ACE2KO hearts in response to DIO. NADPH oxidase activity (*M*), representative DHE staining images (*N*), and quantification of DHE fluorescence (*O*) show increased oxidative stress in ACE2KO-HFD hearts compared with WT-HFD hearts. $n = 12$ (*A–D*); $n = 6$ (*E–H*); $n = 4$ (*I*, *J*, *L*, *N*, *O*); $n = 10$ (*K*, *M*). *$P < 0.05$ compared with the respective CON groups; #$P < 0.05$ compared with the WT-HFD group; \$$P < 0.05$ compared with WT-CON group. Scale bar = 25 μm (*I*) and 100 μm (*N*). A.U., arbitrary unit; p, phosphorylated; R.E., relative expression; R.R., relative ratio; T, total; wt, weight.

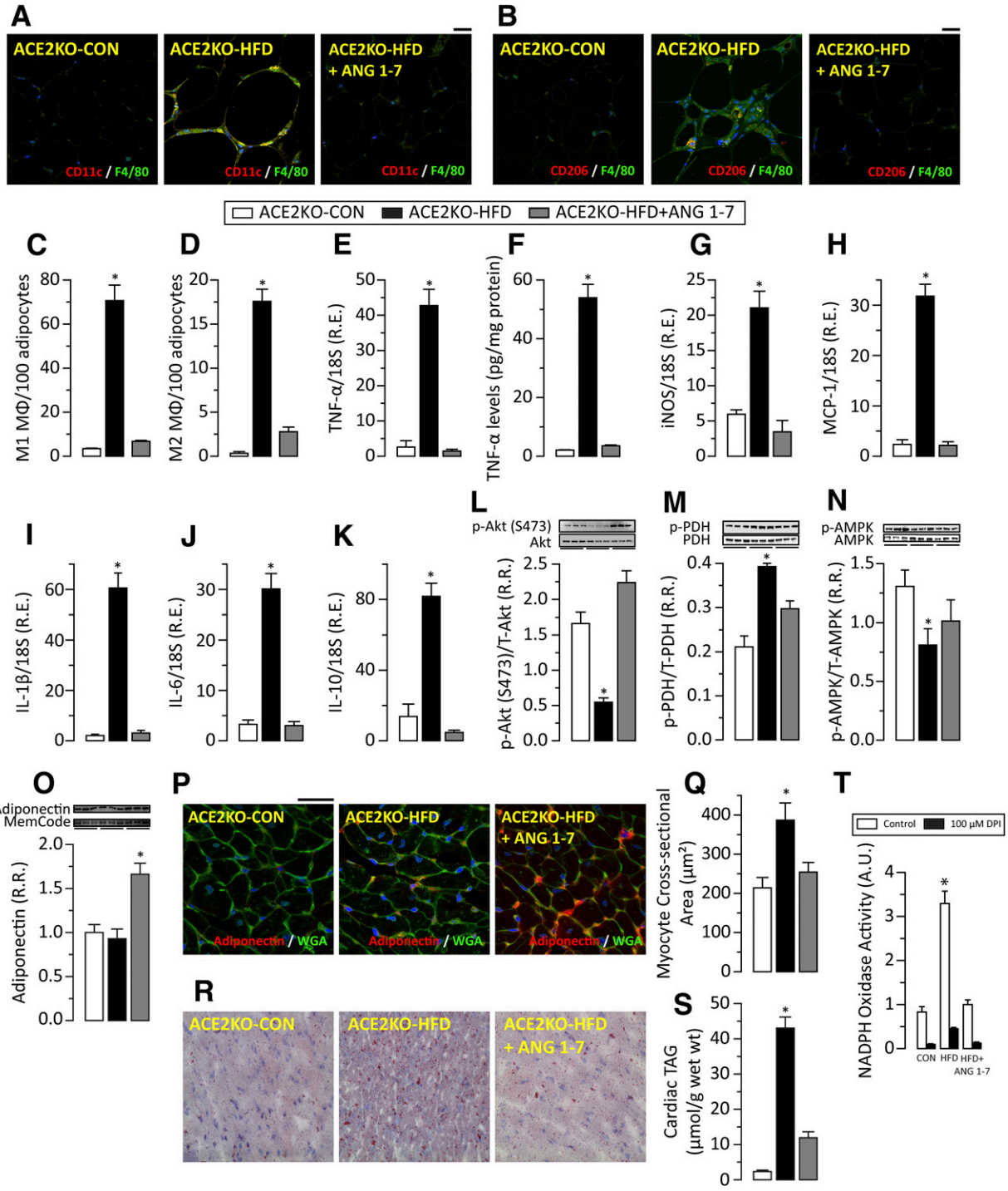

Figure 4—Ang 1-7 treatment ameliorates EAT inflammation, modulates molecular signaling pathways, and decreases cardiac steatosis and oxidative stress, resulting in the prevention of heart failure in ACE2KO-HFD mice. Representative IF images for F4/80 and CD11c (*A*) and CD206 (*B*) and M1 and M2 phenotypes of Mϕ (*C* and *D*) show markedly increased inflammation in the ACE2KO-HFD EAT, whereas Ang 1-7 treatment entirely prevented EAT inflammation (*A*–*D*). Gene expression analysis and ELISA show increased expression of TNF-α [mRNA (*E*) and protein (*F*)], iNOS (*G*), MCP-1 (*H*), IL-1β (*I*), IL-6 (*J*), and IL-10 (*K*) mRNA in ACE2KO-HFD EAT, which was reversed by the Ang 1-7 treatment. Ang 1-7 treatment reversed the changes in the phosphorylation of Akt (*L*), PDH (*M*), and AMPK (*N*) and markedly increased myocardial adiponectin levels as shown by Western blot analysis (*O*) and representative IF images (*P*). Representative WGA staining images (*P*) and myocyte cross-sectional area (*Q*) show Ang 1-7–mediated attenuation of cardiac hypertrophy in ACE2KO-HFD mice. Oil Red O staining revealed decreased intramyocardial lipid accumulation (*R*), and biochemical analysis showed decreased cardiac TAG levels (*S*) in Ang 1-7–treated ACE2KO-HFD hearts. NADPH oxidase activity showed decreased oxidative stress in Ang 1-7–treated ACE2KO-HFD hearts (*T*). $n = 4$ (*A*–*D*, *P*–*R*); $n = 12$ (*E*, *G*–*K*); $n = 8$ (*F*); $n = 6$ (*L*–*O*); $n = 10$ (*S*, *T*). $^*P < 0.05$ compared with all the other groups. Scale bar = 25 μm (*A*, *B*, *P*). A.U., arbitrary unit; DPI, diphenyleneiodonium; p, phosphorylated; R.E., relative expression; R.R., relative ratio; T, total; wt, weight.

Body composition was analyzed by quantitative magnetic resonance, which showed a reduction in fat mass (Supplementary Fig. 6*D*) but not lean mass (Supplementary Fig. 6*E*) in ACE2KO-HFD mice in response to Ang 1-7. Adverse remodeling of EAT in the ACE2KO-HFD group was markedly corrected in response to Ang 1-7, leading to reduced inflammatory cell infiltration and adipocyte size (Supplementary Fig. 4*F–I*) concomitant with reduced $CD11c^+/F4/80^+$ and $CD206^+/F4/80^+$ Mϕ (Fig. 4*A–D*) and decreased expression of pro- and anti-inflammatory cytokines TNF-α (mRNA and protein levels [Fig. 4*E* and *F*]), iNOS, MCP-1, IL-1β, IL-6, and IL-10 (Fig. 4*G–K*). The anti-inflammatory effects closely linked to Ang 1-7 treatment reversed the changes in phosphorylation of Akt (Fig. 4*L*), PDH (Fig. 4*M*), and AMPK (Fig. 4*N*) consistent with improved myocardial response to insulin. Of note, Ang 1-7 treatment markedly increased the myocardial adiponectin levels confirmed by Western blot analysis (Fig. 4*O*) and IF staining (Fig. 4*P*). Assessment of cardiomyocyte cross-sectional area confirmed that Ang 1-7 treatment mediated a reduction in cardiac hypertrophy in ACE2KO-HFD mice (Fig. 4*Q*).

Oil Red O staining (Fig. 4*R*) and biochemical analysis of TAG (Fig. 4*S*) showed that Ang 1-7 treatment also attenuated myocardial lipid accumulation in ACE2KO-HFD hearts, leading to reduced cardiac steatosis (Fig. 4*R* and *S*). Ang 1-7 treatment reduced myocardial oxidative stress and fibrosis as evidenced by decreased NADPH oxidase activity and DHE fluorescence along with reduced myocardial collagen fraction (Fig. 4*T* and Supplementary Fig. 7*A–D*). Ang 1-7–mediated attenuation of EAT inflammation, correction of altered signaling, and reduced lipotoxicity prevented DIO-induced heart failure in the ACE2KO mice and reduced mRNA expression of cardiac disease markers, including ANF, BNP, α-skeletal actin, and β-MHC (Supplementary Fig. 7*E–H*). LV pressure-volume loop analysis (Supplementary Fig. 4*I*) showed reduced LVEDP (Supplementary Fig. 7*J*), suggesting improved diastolic function in the Ang 1-7–treated ACE2KO-HFD mice, which was associated with improved active relaxation (Tau) (Supplementary Fig. 7*K*) and passive stiffness (EDPVR) (Supplementary Fig. 7*L*).

DISCUSSION

Obesity is strongly associated with HFPEF, a condition with high mortality and morbidity and limited therapy (1–4). Rodents exposed to DIO are generally accepted as a valid model to mimic human obesity (5–7). We showed that ACE2 was upregulated in murine and human EAT in association with obesity and cardiac dysfunction. Loss of ACE2 resulted in multifactorial alterations, including pathological hypertrophy, lipotoxicity, and cardiac metabolism, in the setting of EAT inflammation (Supplementary Fig. 8). We found increased glucose intolerance, which has been linked to pathological cardiac hypertrophy (35,36), in ACE2KO-HFD mice despite reduced obesity. DIO in WT mice resulted in increased $CD206^+/F4/80^+$ resident Mϕ in EAT, which was associated with gene expression linked to the M(IL-4) Mϕ phenotype. In contrast, ACE2KO-HFD showed polarization of Mϕ phenotype, resulting in increased resident $CD11c^+/F4/80^+$ Mϕ, which then resulted in increased mRNA expression of proinflammatory cytokines linked with the M(IFN-γ) Mϕ phenotype (Supplementary Fig. 8). Although ACE2 expression in bone marrow can regulate Mϕ polarization and adipose tissue inflammation (37), we show a novel role of ACE2-regulated Mϕ polarization and EAT inflammation in the progression of HFPEF. Of note, human EAT obtained from obese patients with HFPEF also showed a marked increase in EAT inflammation and resident $CD11c^+/F4/80^+$ Mϕ. These results illustrate a fundamental role of Mϕ in adipose tissue inflammation and the regulation of insulin sensitivity (28) as illustrated by the increased insulin sensitivity associated with deletion of M1-mediated inflammatory marker genes (e.g., TNF-α) and the ablation of $CD11c^+$ cells (38,39).

Ang 1-7 treatment prevented DIO-mediated EAT inflammation and cardiac dysfunction in the ACE2 null background. Ang 1-7 effects are predominantly mediated by the activation of its endogenous G-protein–coupled receptor Mas, which is widely expressed (14,40). The current results show a critical role of ACE2 in the regulation of Mϕ phenotypes. Ang II binding and activation of AT1R polarizes Mϕ (41), whereas Ang 1-7/MasR axis activation decreases the expression of the proinflammatory cytokines, including TNF-α and IL-6 (42). By regulating the balance of RAS toward Ang 1-7/MasR axis activation, ACE2 is expected to decrease the polarization of Mϕ. However, the exact mechanism of the role of RAS in Mϕ polarization remains uncertain and warrants detailed investigation.

EAT thickness and inflammation in obesity is associated with the progression of cardiac dysfunction (26,43–45). Common pathways involved in the pathogenesis of obesity and cardiovascular disease include insulin resistance and lipotoxicity. ACE2KO-HFD mice showed increased cardiac steatosis and lipotoxicity in response to DIO. Cardiac steatosis and lipotoxicity are associated with worsening heart failure in obese men without diabetes (26,34). We also found increased myocardial insulin resistance in ACE2KO-HFD hearts, which was associated with worsened global insulin signaling, decreased myocardial adiponectin levels, and decreased phosphorylation of AMPK with associated diastolic dysfunction and heart disease. Myocardial insulin resistance is well known to be associated with the heart failure, although the cause-and-effect relationship in the current study needs further investigation (46). Insulin-perfused ACE2KO-HFD hearts showed decreased phosphorylation of Akt, increased PDK4, and phosphorylation and inactivation of PDH indicative of impaired myocardial insulin signaling resulting in decreased glucose oxidation (47). AMPK acts as a metabolic master switch regulating several intracellular systems, including the cellular uptake of glucose, β-oxidation

of fatty acids, and biogenesis of GLUT4; thus, decreased phosphorylation of AMPK (inactivation) may have contributed to the cardiac insulin resistance in ACE2KO-HFD hearts. Phosphorylation of AMPK in the healthy heart is partly regulated by adiponectin, an adipokine exclusively produced in the adipocytes (32,48). Adiponectin is important for maintaining heart function in the setting of DIO (33). The present observation of reduced myocardial adiponectin in the ACE2KO-HFD model may be an important link between the pathological remodeling of EAT and adverse effects on the heart. Of note, ACE2KO-HFD hearts showed a greater increase in impaired active relaxation with equivalent passive stiffness than did the WT-HFD hearts, which could be attributed to enhanced metabolic dysfunction and equivalent fibrosis in these hearts. Of note, Ang 1-7 treatment reversed pathological changes observed in ACE2KO-HFD EAT and hearts. These results are consistent with a pivotal role of the ACE2/Ang 1-7 axis in cardiovascular (13,21) and diabetic kidney (49,50) diseases.

The current data show that Ang 1-7–mediated cardioprotection against obesity-induced cardiac dysfunction is multifactorial and mediated by improved molecular signaling and decreased myocardial fibrosis, lipotoxicity, and EAT inflammation. Ang 1-7 reduces glucose intolerance and insulin resistance and prevents diabetic cardiomyopathy in the obese type 2 diabetic model (13,51). The results illustrate novel effects of Ang 1-7 in increasing myocardial adiponectin levels and mediating anti-inflammatory effects on EAT and beneficial effects on heart function.

In conclusion, we found a novel role of ACE2 in obesity where ACE2 negatively regulates obesity-induced EAT inflammation, cardiac insulin resistance, and alterations in cardiac metabolism. Of note, Ang 1-7 treatment improves glucose intolerance, EAT inflammation, and cardiac insulin resistance and prevents the HFPEF phenotype in DIO. Enhancing ACE2 or Ang 1-7 action represents a potential therapeutic option for obesity and its associated heart disease.

Funding. V.B.P. and N.P. are supported by Alberta Innovates-Health Solutions (AI-HS) and Heart and Stroke Foundation (HSF) postdoctoral fellowships. B.A.M. and S.K.D. are supported by AI-HS graduate studentships. Funding support was also provided by the Canadian Institutes of Health Research, HSF, AI-HS, and the National Institutes of Health.

Duality of Interest. No potential conflicts of interest relevant to this article were reported.

Author Contributions. V.B.P. designed the research, conducted the experiments, analyzed data, performed the statistical analysis, and wrote the manuscript. J.M., B.A.M., R.B., S.K.D., T.R., and N.P. conducted the experiments. J.M.P. and M.B.G. provided new reagents, analytical tools, and mice and analyzed data. G.D.L. provided new reagents, analytical tools, and mice; analyzed data; and wrote the manuscript. G.Y.O. designed the research, analyzed data, performed the statistical analysis, and wrote the manuscript. G.Y.O. is the guarantor of this work and, as such, had full access to all the data in the study and takes responsibility for the integrity of the data and the accuracy of the data analysis.

References

1. Kenchaiah S, Sesso HD, Gaziano JM. Body mass index and vigorous physical activity and the risk of heart failure among men. Circulation 2009;119:44–52
2. Kenchaiah S, Evans JC, Levy D, et al. Obesity and the risk of heart failure. N Engl J Med 2002;347:305–313
3. Owan TE, Hodge DO, Herges RM, Jacobsen SJ, Roger VL, Redfield MM. Trends in prevalence and outcome of heart failure with preserved ejection fraction. N Engl J Med 2006;355:251–259
4. Yancy CW, Jessup M, Bozkurt B, et al. 2013 ACCF/AHA guideline for the management of heart failure: executive summary: a report of the American College of Cardiology Foundation/American Heart Association Task Force on practice guidelines. Circulation 2013;128:1810–1852
5. Sparks LM, Xie H, Koza RA, et al. A high-fat diet coordinately downregulates genes required for mitochondrial oxidative phosphorylation in skeletal muscle. Diabetes 2005;54:1926–1933
6. Boudina S, Han YH, Pei S, et al. UCP3 regulates cardiac efficiency and mitochondrial coupling in high fat-fed mice but not in leptin-deficient mice. Diabetes 2012;61:3260–3269
7. Boudina S, Sena S, Theobald H, et al. Mitochondrial energetics in the heart in obesity-related diabetes: direct evidence for increased uncoupled respiration and activation of uncoupling proteins. Diabetes 2007;56:2457–2466
8. Paul M, Poyan Mehr A, Kreutz R. Physiology of local renin-angiotensin systems. Physiol Rev 2006;86:747–803
9. Jones BH, Standridge MK, Moustaid N. Angiotensin II increases lipogenesis in 3T3-L1 and human adipose cells. Endocrinology 1997;138:1512–1519
10. Boschmann M, Ringel J, Klaus S, Sharma AM. Metabolic and hemodynamic response of adipose tissue to angiotensin II. Obes Res 2001;9:486–491
11. Tipnis SR, Hooper NM, Hyde R, Karran E, Christie G, Turner AJ. A human homolog of angiotensin-converting enzyme. Cloning and functional expression as a captopril-insensitive carboxypeptidase. J Biol Chem 2000;275:33238–33243
12. Donoghue M, Hsieh F, Baronas E, et al. A novel angiotensin-converting enzyme-related carboxypeptidase (ACE2) converts angiotensin I to angiotensin 1-9. Circ Res 2000;87:E1–E9
13. Mori J, Patel VB, Abo Alrob O, et al. Angiotensin 1-7 ameliorates diabetic cardiomyopathy and diastolic dysfunction in db/db mice by reducing lipotoxicity and inflammation. Circ Heart Fail 2014;7:327–339
14. Loot AE, Roks AJ, Henning RH, et al. Angiotensin-(1-7) attenuates the development of heart failure after myocardial infarction in rats. Circulation 2002;105:1548–1550
15. Zisman LS, Meixell GE, Bristow MR, Canver CC. Angiotensin-(1-7) formation in the intact human heart: in vivo dependence on angiotensin II as substrate. Circulation 2003;108:1679–1681
16. Patel VB, Takawale A, Ramprasath T, et al. Antagonism of angiotensin 1-7 prevents the therapeutic effects of recombinant human ACE2. J Mol Med (Berl) 2015;93:1003–1013
17. Gupte M, Boustany-Kari CM, Bharadwaj K, et al. ACE2 is expressed in mouse adipocytes and regulated by a high-fat diet. Am J Physiol Regul Integr Comp Physiol 2008;295:R781–R788
18. Patel VB, Bodiga S, Basu R, et al. Loss of angiotensin-converting enzyme-2 exacerbates diabetic cardiovascular complications and leads to systolic and vascular dysfunction: a critical role of the angiotensin II/AT1 receptor axis. Circ Res 2012;110:1322–1335
19. Patel VB, Parajuli N, Oudit GY. Role of angiotensin-converting enzyme 2 (ACE2) in diabetic cardiovascular complications. Clin Sci (Lond) 2014;126:471–482
20. Patel VB, Zhong JC, Fan D, et al. Angiotensin-converting enzyme 2 is a critical determinant of angiotensin II-induced loss of vascular smooth muscle cells and adverse vascular remodeling. Hypertension 2014;64:157–164
21. Zhong J, Basu R, Guo D, et al. Angiotensin-converting enzyme 2 suppresses pathological hypertrophy, myocardial fibrosis, and cardiac dysfunction. Circulation 2010;122:717–728

22. Patel VB, Bodiga S, Fan D, et al. Cardioprotective effects mediated by angiotensin II type 1 receptor blockade and enhancing angiotensin 1-7 in experimental heart failure in angiotensin-converting enzyme 2-null mice. Hypertension 2012;59:1195–1203
23. Patel VB, Wang Z, Fan D, et al. Loss of p47phox subunit enhances susceptibility to biomechanical stress and heart failure because of dysregulation of cortactin and actin filaments. Circ Res 2013;112:1542–1556
24. Fan W, Cheng K, Qin X, et al. mTORC1 and mTORC2 play different roles in the functional survival of transplanted adipose-derived stromal cells in hind limb ischemic mice via regulating inflammation in vivo. Stem Cells 2013;31:203–214
25. Takeda M, Yamamoto K, Takemura Y, et al. Loss of ACE2 exaggerates high-calorie diet-induced insulin resistance by reduction of GLUT4 in mice. Diabetes 2013;62:223–233
26. Van Gaal LF, Mertens IL, De Block CE. Mechanisms linking obesity with cardiovascular disease. Nature 2006;444:875–880
27. Strissel KJ, Stancheva Z, Miyoshi H, et al. Adipocyte death, adipose tissue remodeling, and obesity complications. Diabetes 2007;56:2910–2918
28. Fujisaka S, Usui I, Bukhari A, et al. Regulatory mechanisms for adipose tissue M1 and M2 macrophages in diet-induced obese mice. Diabetes 2009;58:2574–2582
29. Murray PJ, Allen JE, Biswas SK, et al. Macrophage activation and polarization: nomenclature and experimental guidelines. Immunity 2014;41:14–20
30. Huss JM, Kelly DP. Mitochondrial energy metabolism in heart failure: a question of balance. J Clin Invest 2005;115:547–555
31. Houtkooper RH, Pirinen E, Auwerx J. Sirtuins as regulators of metabolism and healthspan. Nat Rev Mol Cell Biol 2012;13:225–238
32. Ouchi N, Parker JL, Lugus JJ, Walsh K. Adipokines in inflammation and metabolic disease. Nat Rev Immunol 2011;11:85–97
33. Guo R, Zhang Y, Turdi S, Ren J. Adiponectin knockout accentuates high fat diet-induced obesity and cardiac dysfunction: role of autophagy. Biochim Biophys Acta 2013;1832:1136–1148
34. Granér M, Siren R, Nyman K, et al. Cardiac steatosis associates with visceral obesity in nondiabetic obese men. J Clin Endocrinol Metab 2013;98:1189–1197
35. Capaldo B, Di Bonito P, Iaccarino M, et al. Cardiovascular characteristics in subjects with increasing levels of abnormal glucose regulation: the Strong Heart Study. Diabetes Care 2013;36:992–997
36. Rutter MK, Parise H, Benjamin EJ, et al. Impact of glucose intolerance and insulin resistance on cardiac structure and function: sex-related differences in the Framingham Heart Study. Circulation 2003;107:448–454
37. Thatcher SE, Gupte M, Hatch N, Cassis LA. Deficiency of ACE2 in bone-marrow-derived cells increases expression of TNF-alpha in adipose stromal cells and augments glucose intolerance in obese C57BL/6 mice. Int J Hypertens 2012;2012:762094
38. Patsouris D, Li PP, Thapar D, Chapman J, Olefsky JM, Neels JG. Ablation of CD11c-positive cells normalizes insulin sensitivity in obese insulin resistant animals. Cell Metab 2008;8:301–309
39. Uysal KT, Wiesbrock SM, Marino MW, Hotamisligil GS. Protection from obesity-induced insulin resistance in mice lacking TNF-alpha function. Nature 1997;389:610–614
40. Santos RA, Simoes e Silva AC, Maric C, et al. Angiotensin-(1-7) is an endogenous ligand for the G protein-coupled receptor Mas. Proc Natl Acad Sci U S A 2003;100:8258–8263
41. Yamamoto S, Yancey PG, Zuo Y, et al. Macrophage polarization by angiotensin II-type 1 receptor aggravates renal injury-acceleration of atherosclerosis. Arterioscler Thromb Vasc Biol 2011;31:2856–2864
42. Souza LL, Costa-Neto CM. Angiotensin-(1-7) decreases LPS-induced inflammatory response in macrophages. J Cell Physiol 2012;227:2117–2122
43. Cherian S, Lopaschuk GD, Carvalho E. Cellular cross-talk between epicardial adipose tissue and myocardium in relation to the pathogenesis of cardiovascular disease. Am J Physiol Endocrinol Metab 2012;303:E937–E949
44. Fontes-Carvalho R, Fontes-Oliveira M, Sampaio F, et al. Influence of epicardial and visceral fat on left ventricular diastolic and systolic functions in patients after myocardial infarction. Am J Cardiol 2014;114:1663–1669
45. Fitzgibbons TP, Czech MP. Epicardial and perivascular adipose tissues and their influence on cardiovascular disease: basic mechanisms and clinical associations. J Am Heart Assoc 2014;3:e000582
46. Ashrafian H, Frenneaux MP, Opie LH. Metabolic mechanisms in heart failure. Circulation 2007;116:434–448
47. Mori J, Basu R, McLean BA, et al. Agonist-induced hypertrophy and diastolic dysfunction are associated with selective reduction in glucose oxidation: a metabolic contribution to heart failure with normal ejection fraction. Circ Heart Fail 2012;5:493–503
48. Liao Y, Takashima S, Maeda N, et al. Exacerbation of heart failure in adiponectin-deficient mice due to impaired regulation of AMPK and glucose metabolism. Cardiovasc Res 2005;67:705–713
49. Tikellis C, Bialkowski K, Pete J, et al. ACE2 deficiency modifies renoprotection afforded by ACE inhibition in experimental diabetes. Diabetes 2008;57:1018–1025
50. Oudit GY, Liu GC, Zhong J, et al. Human recombinant ACE2 reduces the progression of diabetic nephropathy. Diabetes 2010;59:529–538
51. Marcus Y, Shefer G, Sasson K, et al. Angiotensin 1-7 as means to prevent the metabolic syndrome: lessons from the fructose-fed rat model. Diabetes 2013;62:1121–1130